Supplementary Material for:

Canopy structure, topography and weather are equally important drivers of small-scale snow cover dynamics in sub-alpine forests

Giulia Mazzotti[1,2], Clare Webster[1,3], Louis Quéno[1], Bertrand Cluzet[1], Tobias Jonas[1]

[1]WSL Institute for Snow and Avalanche Research SLF, 7260 Davos Dorf, Switzerland
[2]Univ. Grenoble Alpes, Université de Toulouse, Météo-France, CNRS, CNRM, Centre d'Études de la Neige, 38100 St. Martin d'Hères, France
[3]Department of Geosciences, University of Oslo, 0316 Oslo, Norway

Contents:

S1: Meteorological conditions during the simulation period

The following figures provide an overview of meteorological conditions during the six simulated water years to give context to the observed differences in snow cover dynamics outlined in the main article. We focus on the three variables that, as elaborated on in the main article, have the largest potential to cause differences between years: snowfall (affects total accumulation), shortwave radiation, and temperature (affect the timing and strength of melt, as well as whether it is mainly driven by short- or longwave radiation contributions). The left panel of Figure S1.1 reports weekly snowfall sums between the beginning of November and June, which represent the earliest and latest yearly median of the start of snow cover period and snow disappearance date. Some marked differences in how the precipitation is distributed throughout the snow season can be observed. The right panel of Figure S1.1 shows cumulative snowfall between the median start of snow cover and snow disappearance dates of each specific year. This visualization evidences the substantial differences in timing and length of snow cover period and total snowfall between the years, with WY2016 (lowest accumulation) amounting to only half of total snowfall of WY 2019 (highest accumulation).

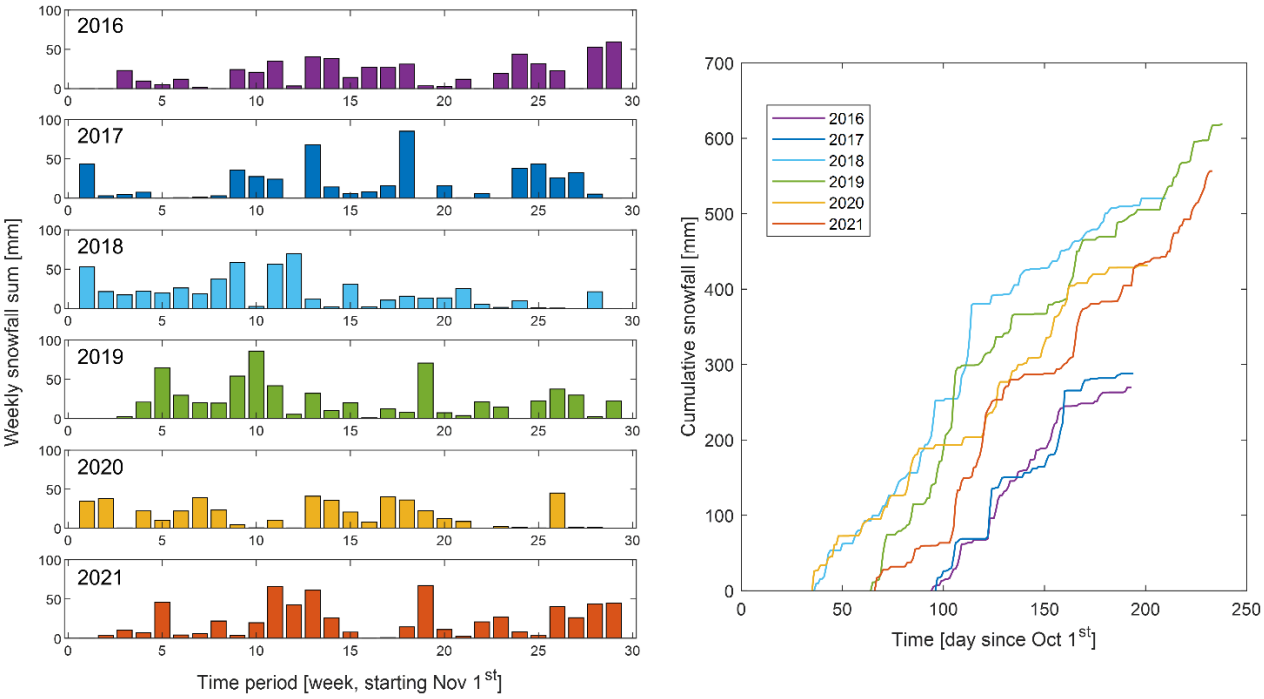

Figure S1.1: Weekly snowfall during the six modelled winters between November and June (left) and cumulative snowfall over the median snow cover duration period of the respective year (right).

Figure S1.2 contrasts shortwave radiation (left) and air temperatures (right) during the six simulated winters, with the upper row showing weekly values and the lower row the weekly deviation from the six-year average. While no year is clearly above or below average for any of the two variables for the entire season, some marked deviations from the averages can be detected in these plots, for instance the relatively warm period in the middle of the 2020 winter.

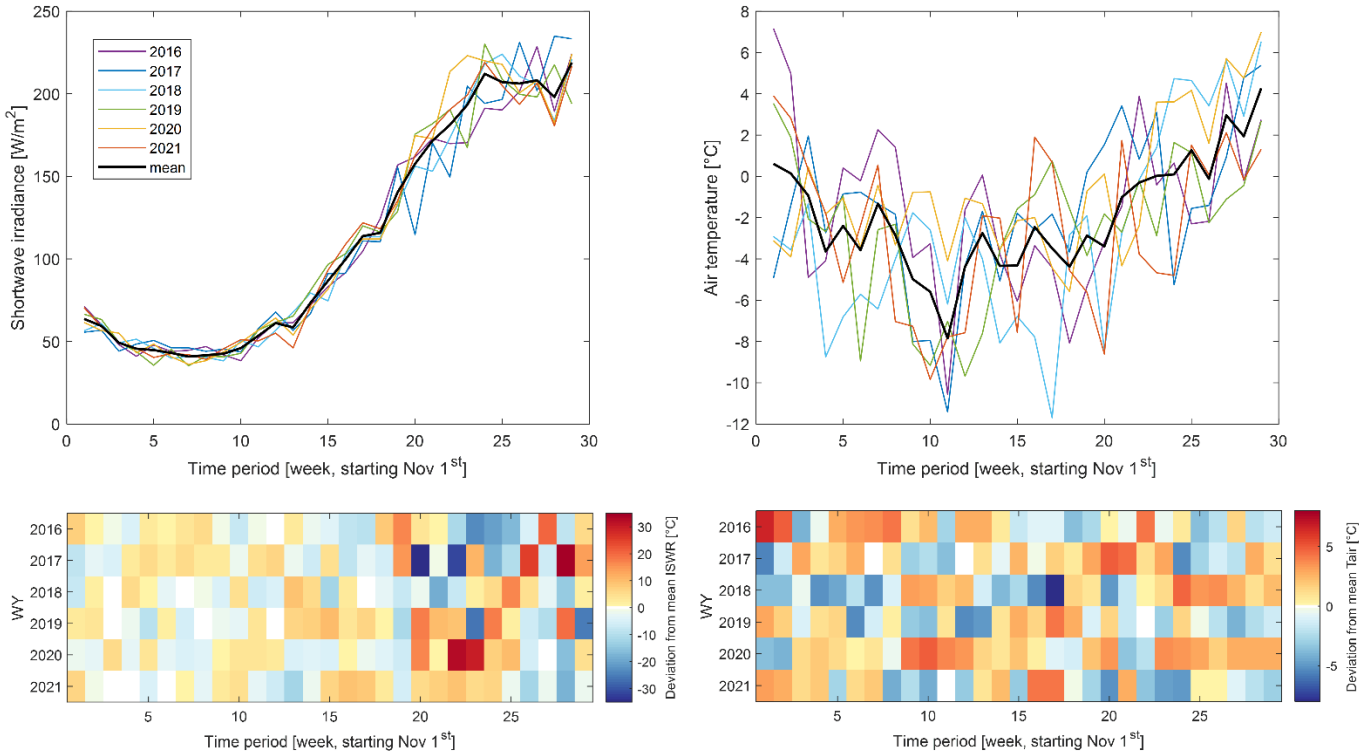

Figure S1.2: Incoming shortwave radiation (left) and air temperature (top right) of the six simulated winters, and deviation from mean (lower row) for the same variables.

S2: Maps of snow cover and energy balance descriptors over the full model domain

While some figures in the main article include maps of a subdomain of the model domain to illustrate patterns of snow cover descriptors and energy fluxes, here we add the corresponding maps for the full model domain for interested readers. Maps of local canopy cover fraction and the DEM are included for reference in Figure S2.1, as in Figure 5 of the main article. Figure 2.2 reports peak SWE, ablation rate, day of peak SWE and snow disappearance day for WY 2019, corresponding to Figure 5 of the main article. Figure S2.3 shows average incoming irradiances and early melt between mid-January and end of February 2019, analogous to Figure 7 of the main article. Note the addition of incoming longwave radiation which further underpins the statement that all-wave irradiance patterns are largely determined by patterns of incoming shortwave radiation. Figure S2.4 includes average patterns of the individual surface energy balance components (net short- and longwave radiation, sensible and latent heat) as well as net surface energy flux computed as the sum of the four. Maps shown are for the second half of February 2019, analogous to the upper part of Figure 8 in the main article.

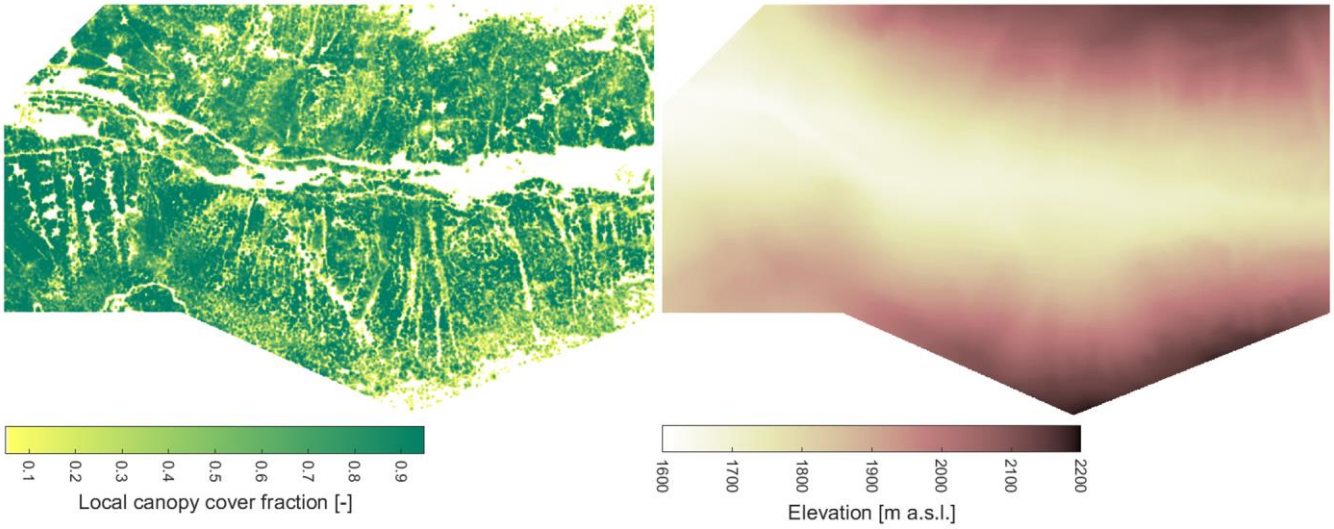

Figure S2.1: Local canopy cover fraction (left) and elevation (right) across the full model domain.

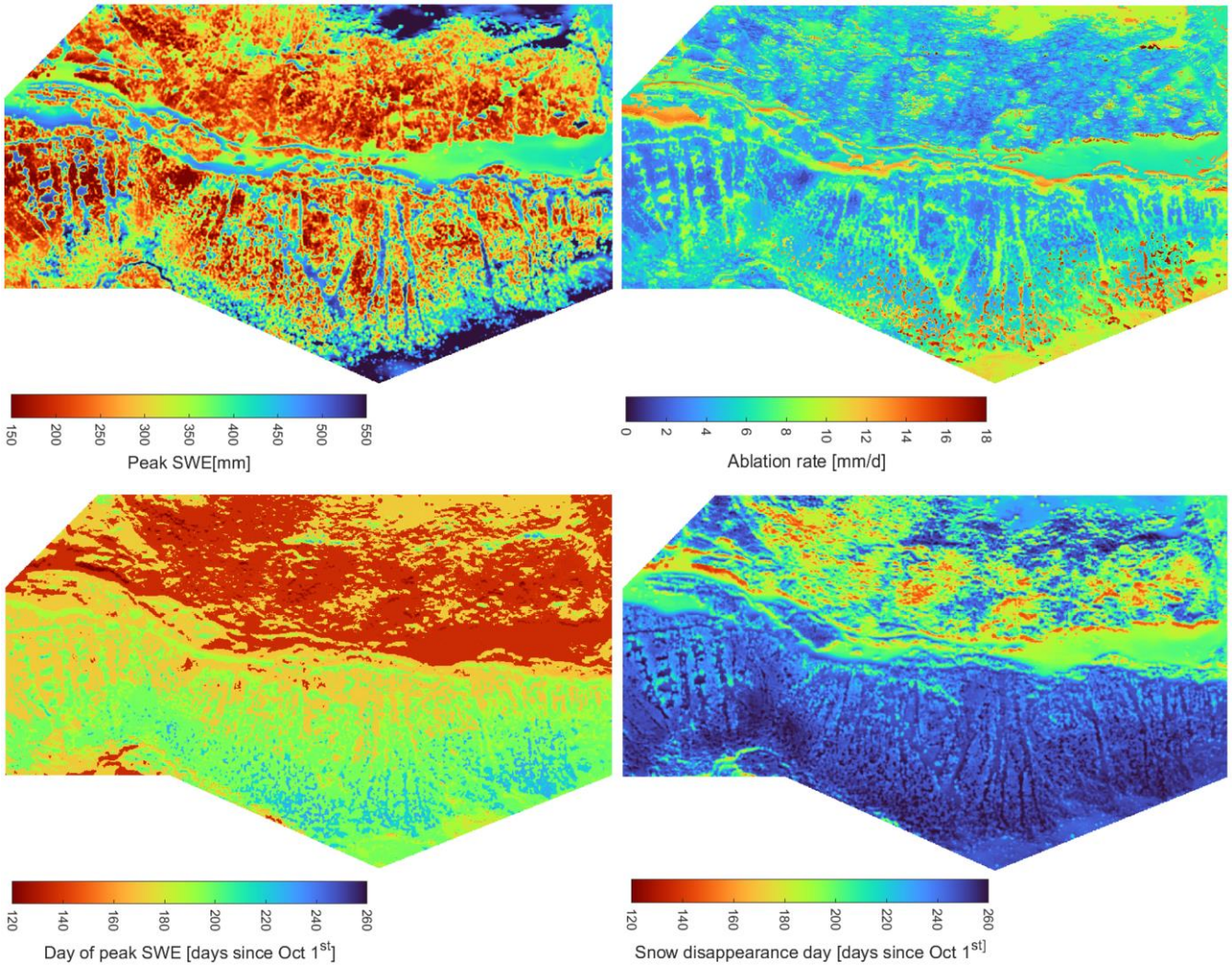

Figure S2.2: Peak SWE, ablation rate, day of peak SWE and snow disappearance day in WY 2019

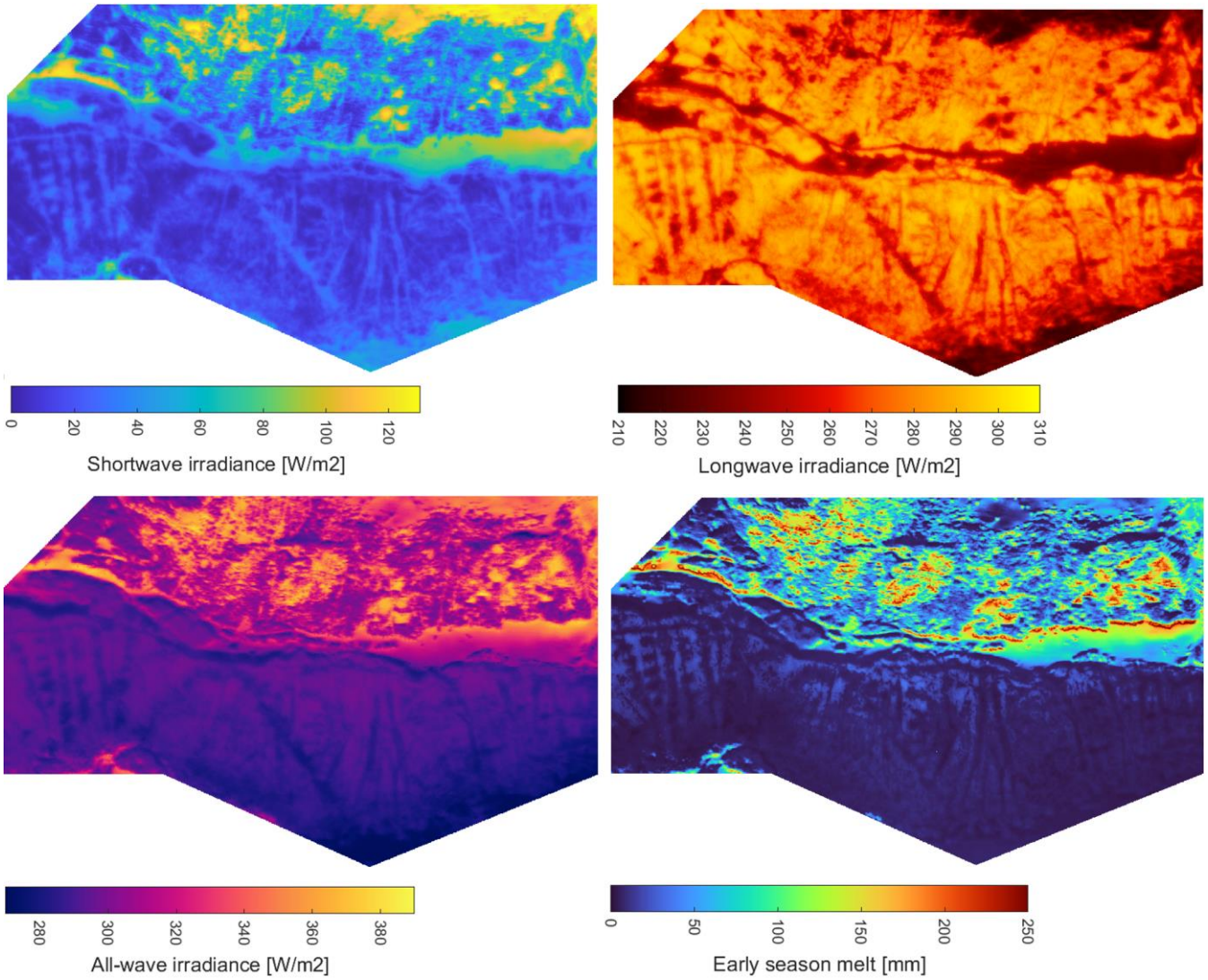

Figure S2.3: Average incoming short and longwave radiation, all-wave radiation and snow melt between mid-January and end of February 2019

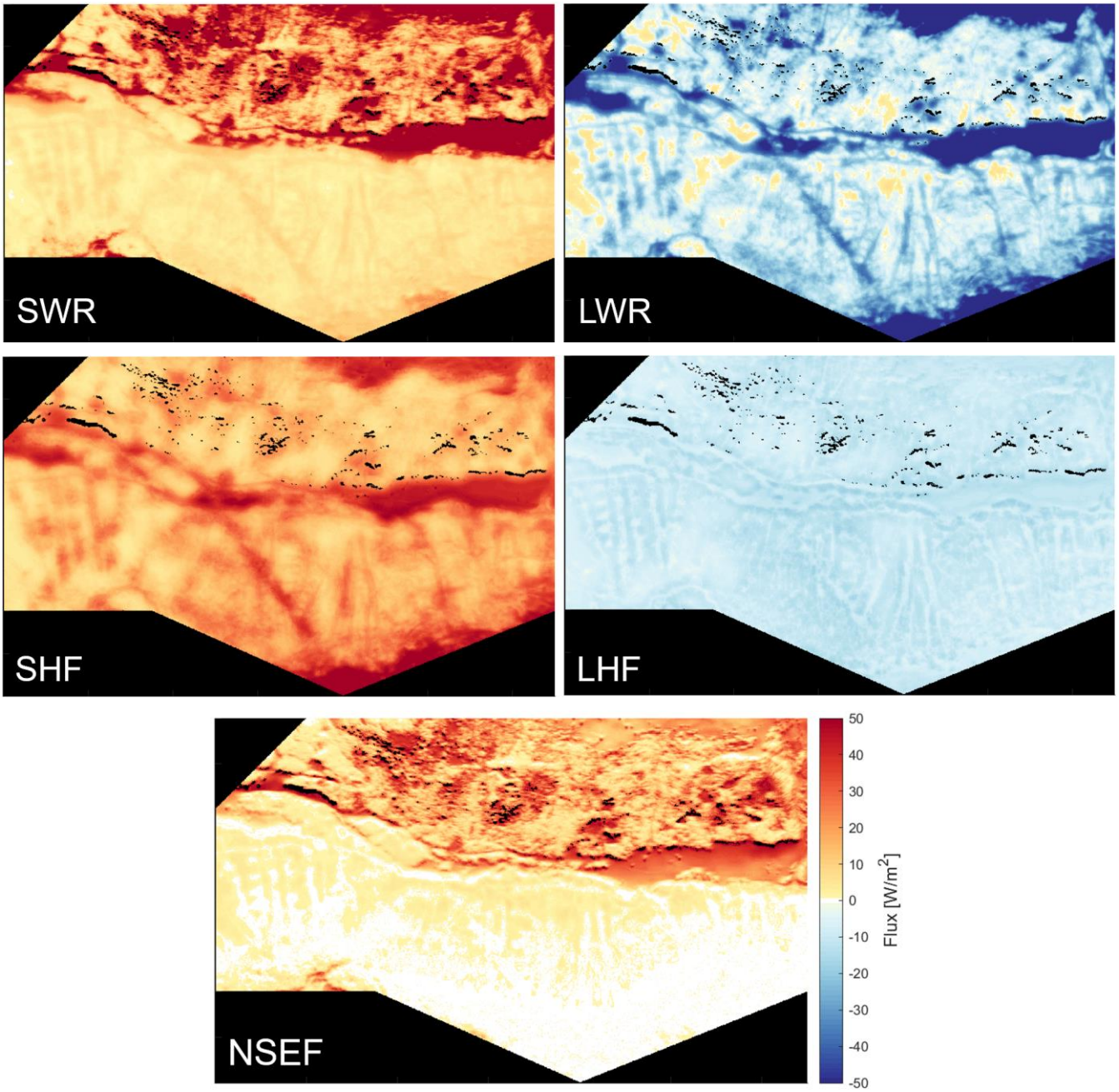

Figure S2.4: Individual surface energy components (net short- and wave radiation, SWR and LWR, as well as sensible and latent heat fluxes, SHF and LHF) and net surface energy flux (NSEF) computed as sum of the four, for the second half of February 2019.

S3: Location of example points within the model domain

The location of example points used for the analysis of snow evolution and energy balance partitioning pathways presented in Section 3.3 and 3.5 are shown in Figure S3.1. In Section 3.3, points were chosen to cover the entire range of canopy structures and topographic locations (Figure S3.1b, corresponding to points shown in Figure 6 of the main article). In Section 3.5, we focused our analysis on points located at the south-exposed slope and sparse canopy or small gaps to explore differences between years (Figure S3.1c, corresponding to points shown in Figure 10 of the main article).

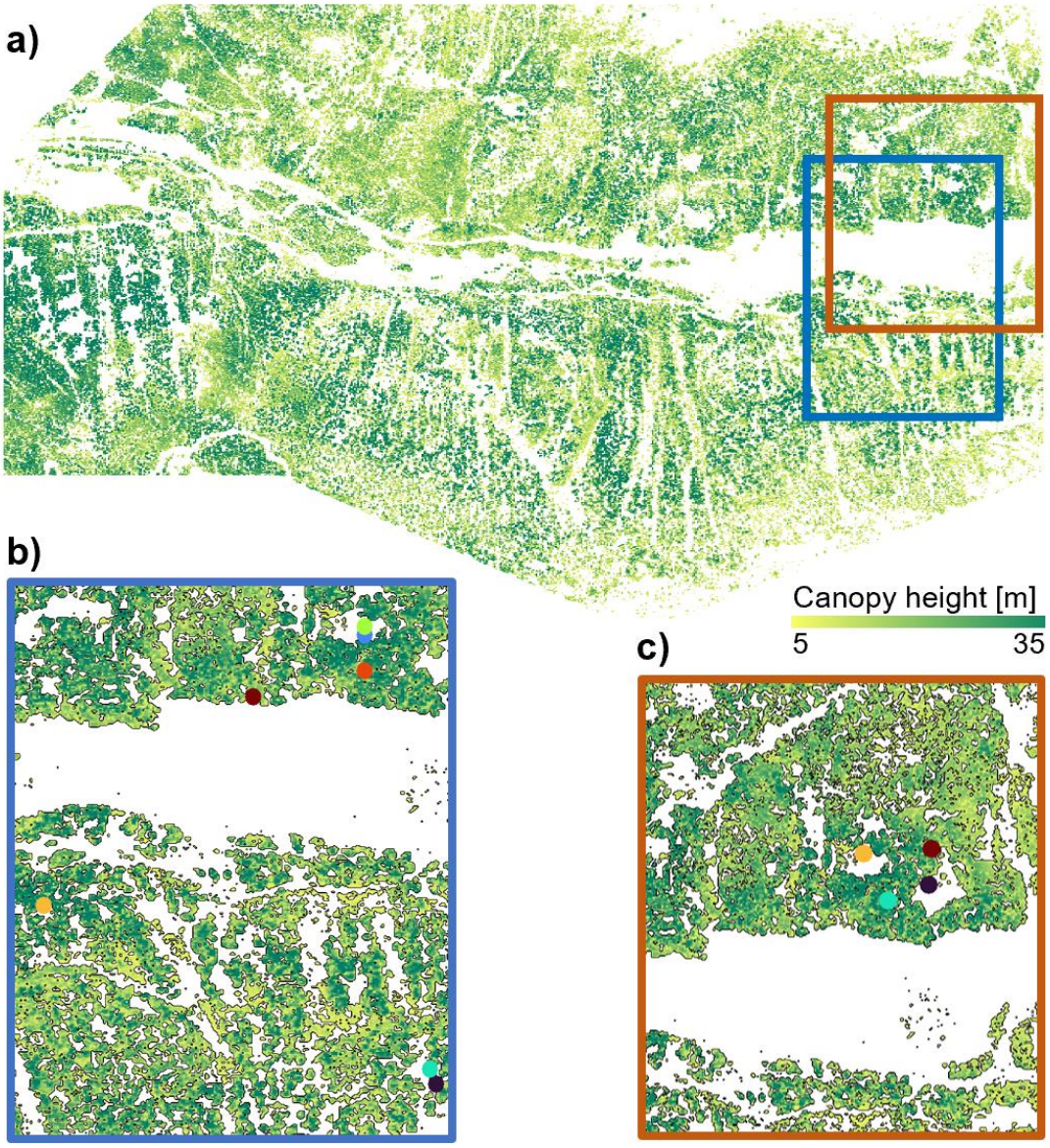

Figure S3.1: Locations of example points. Overview (a), points presented in Section 3.3 / Figure 6 of the main article (b), and points used in Section 3.5 / Figure 10 of the main article. Colours marking individual points match the colour code of the figures in the main article.